A Combined Experimental and Modeling Study on Isopropyl Nitrate Pyrolysis

Nicolas Vin, Hans-Heinrich Carstensen, Olivier Herbinet, Jérémy Bourgalais, María Ujué Alzueta, Frédérique Battin-Leclerc

A Combined Experimental and Modeling Study on Isopropyl Nitrate Pyrolysis

Nicolas Vin[1,#], Hans-Heinrich Carstensen[2,3], Olivier Herbinet[1,*], Jérémy Bourgalais[1], María Ujué Alzueta[4], Frédérique Battin-Leclerc[1]

[1]Université de Lorraine, CNRS, LRGP, Nancy, 54000, France.
[2]Fundación Agencia Aragonesa para la Investigación y el Desarrollo (ARAID), Zagaroza, 50018, Spain
[3]Escuela de Ingeniería y Arquitectura, Universidad de Zaragoza, Zaragoza, 50018, Spain
[4]Aragón Institute of Engineering Research (I3A), Zaragoza, 50018, Spain

Published in J Phys Chem A (2023) 127, 9, 2123–2135

10.1021/acs.jpca.2c06708

Abstract

Alkyl nitrates thermally decompose by homolytic cleavage of the weak nitrate bond at very low temperatures (e.g. around 500 K at reaction times of a few seconds). This provides the opportunity to study the subsequent chemistry of the initially formed radical (or its subsequent pyrolysis products, if unstable) and nitrogen dioxide at such mild conditions. In this work this idea is applied to isopropyl nitrate (iPN) pyrolysis, which is studied in a tubular reactor at atmospheric pressure, temperatures ranging from 373 K to 773 K and residence times of around 2 s. At the experimental conditions, iPN decomposition starts at 473 K with O-N bond fission producing isopropoxy radical (i-C_3H_7O) and NO_2. i-C_3H_7O is rapidly converted to acetaldehyde (CH_3CHO), which is the most abundant product detected, and methyl radicals. Other major products detected are formaldehyde (CH_2O), methanol (CH_3OH), nitromethane (CH_3NO_2), NO, methane, formamide ($CHONH_2$), and methyl nitrite (CH_3ONO). Four literature nitrogen chemistry models – three of those augmented with iPN specific reactions – have been tested for their ability to predict the iPN decomposition and product profiles. The mechanism by the Curran group performs best but it still under-predicts the observed high formaldehyde and methanol yields. A rate analysis indicates that the branching ratio of the reaction between methyl radicals and nitrogen dioxide is of significant importance. Based on recent theoretical and experimental data, new rate expressions for the two reactions $CH_3+NO_2 \rightarrow CH_3O+NO$ and $CH_3+NO_2+He \rightarrow CH_3ONO_2+He$ are calculated and incorporated in the kinetic models. It is shown that this change clearly improves the predictions, although additional work is needed to achieve good agreement between calculated and measured species profiles.

[*] Corresponding author: olivier.herbinet@univ-lorraine.fr

Introduction

Monopropellants are substances that undergo exothermic decomposition without the need of a separate oxidizer. They are used to provide high levels of thrust for space vehicles or they can be used as power sources in underwater applications[1] but also as additive to improve the cetane number.[2] While 2-ethylhexylnitrate is arguably the most studied additive, there is also substantial interest in isopropyl nitrate (iPN). iPN, a colorless liquid, is a promising "green" monopropellant, which has many economic, health and technical advantages over conventional monopropellant fuels such as hydrazine (N_2H_4) and its derivatives. It is non-toxic and non-corrosive, can be produced at low cost and has low susceptibility towards premature detonation.[3] Blends of iPN with diesel fuel have been used and studied as cetane improver.[4,5] IPN can also be considered as a surrogate to model the thermal destruction of explosives such as trinitrotoluene, octogene or pentaerythritol tetranitrate.[6]

Numerous experimental studies on the thermal decomposition of iPN have been reported in the past. They include experiments with shock tubes,[7-11] rapid compression machines,[12,13] flow and closed cells,[10,14-17] and flames.[18,19] Theoretical and modeling investigations are also known.[11,19] The experiments conducted over a wide range of temperatures, pressures and compositions demonstrated that, like other organic nitrate,[20] the thermal decomposition of iPN proceeds by a well-known bond fission mechanism. Breaking of the weak (around 40 kcal/mol) nitrate bond leads to the formation of NO_2 and an alkoxy radical, isopropoxy (i-C_3H_7O or C_2COJ, "J" denotes the radical site) in the case of iPN.

While the initiation step is well established, the subsequent reactions leading to the observed final products are less well understood. Although an alkoxy radical can undergo a number of competing reaction pathways, the isopropoxy radical is expected to almost exclusively form a methyl radical CH_3 and the carbonyl compound acetaldehyde (CH_3CHO).[17] Thus, the observed species distribution depends on the subsequent interactions between iPN, acetaldehyde, methyl and NO_2. The prediction of the formation of many of the observed products such as nitromethane (CH_3NO_2), NO, formaldehyde (CH_2O), methanol (CH_3OH), water, CO_2 and their yields as a function of temperature requires that all important reactions of the initial products are identified and that accurate rate coefficients for those have been assigned.

To the best of our knowledge, only one kinetic iPN model is currently available in the literature. It has been developed and iteratively optimized by Fuller et al.[11] to interpret shock tube Schlieren studies in a temperature range 700 – 1000 K. In a later study by the same group,[19] this model was slightly modified and applied to ignition delay and flame speed experiments for which good agreements were found. This model so far has not been validated against iPN thermolysis data at temperatures in the 400 – 700 K range.

This current study reports on an experimental investigation of iPN pyrolysis in a tubular reactor at low temperatures (373 K -773 K) and provides quantitative specification of many, though not all products. It constitutes the first study at atmospheric pressure in a flow tube, extending the existing experimental database for this molecule. The measured iPN consumption and product yields are compared to predictions of the iPN model by Fuller et al.[11,19] as well as three additional nitrogen chemistry models, which were augmented with a small iPN sub-mechanism developed as part of this work at the G4 level of theory. The comparisons are used to identify the most important reactions and assess the impact of small uncertainties in the rate expressions on the model predictions. Suggestions to develop an improved kinetic model are made.

Methods

This section of the paper contains the description of the experimental procedure used to obtain iPN pyrolysis data, as well as the methodology used to calculate rate coefficients incorporated in models and to run simulations.

1. Experimental Setup Description

The experimental setup has already been described in a previous study on the pyrolysis of nitromethane[21] and only a brief description with a focus on the specifics related to this work is given here. Experiments were carried out in a tubular reactor at a constant pressure of 1.07 bar, an inlet iPN mole fraction of 0.01 (high dilution in helium). Helium (purity of 99.999%) and iPN (purity of 98%) were purchased from Messer and Sigma-Aldrich, respectively. The gas flow rates were controlled by mass flow controllers (0.5% uncertainty) and the liquid flow rate by a Coriolis flow controller. The tubular reactor is a recrystallized alumina tube with an inner diameter of 20 mm, an outer diameter of 25 mm and a volume of a 294 cm^3. It is heated by an electrical furnace from Vecstar. Temperature gradients along the reactor were measured for several set point temperatures using a S-type thermocouple with a relative uncertainty of 0.5%. These temperature profiles are provided in Figure S1 of the Supporting Material (SM) and were used for running more accurate simulations. At the operating conditions of this study, the reactor can be approximated as plug flow reactor.[22] The evolution of the product mole fractions was measured over a temperature range from 373 to 773 K. The residence time of the gas in the hot zone of the reactor was kept constant at around 2 s at the set-point temperature. Mole changes during the reaction but also the non-isothermal temperature profiles introduce uncertainties in the residence times of several percent.

Species were sampled at the outlet and analyzed by gas chromatography and by Fourier-Transform Infrared (FTIR) spectroscopy (10-meter path cell). A heated transfer line maintained at 433 K was used for sampling to avoid product condensation between the reactor outlet and the analytical devices. A gas chromatograph equipped with a six-port sampling and switching valve, a split injector, a Plot-Q capillary column, a thermal conductivity detector (TCD) and a flame ionization detector (FID) was used for the quantification of light products and the reactant.[22] The identification of the products was achieved with a gas chromatograph coupled to a quadrupole mass spectrometer. Response factors for the FID and the TCD were determined by either injecting calibration mixtures or by using the effective carbon number method (only for the FID). Relative uncertainties in mole fractions are estimated to be less than 10% in most cases but can be higher e.g. for aldehydes. A FTIR apparatus was used to identify and quantify CH_2O, CO, H_2O, HCN, NO, CO_2 and CH_3OH. FTIR calibrations were obtained by injecting standards. The relative uncertainties of the FTIR data are slightly higher than those obtained by GC since interferences may occur between bands of absorbing species. The calculated elemental balances (Figure S2 in SM) show deviations of up to about + 20% for "C", "H" and "O" and -30 % for "N". Missing "N" can be explained by species like molecular nitrogen, which has been detected but not quantified. The excess of the other elements reflects the difficulty in studying the highly reactive iPN at the current conditions.

2. Theoretical Calculations

The CBS-QB3, G4 and CCSD(T) levels of theory as implemented in the Gaussian G16 suite of programs[23] were used to calculate thermochemical parameters related to iPN decomposition chemistry. Electronic energies at the CBS-QB3 and G4 levels were converted with the atomization method to enthalpies of formation. Thermal enthalpy contributions, entropies and heat capacities were calculated with methods from statistical mechanics using the harmonic oscillator-rigid rotor assumption except for internal rotations which are separately evaluated as one-dimensional internal rotors with effective rotational constants.[24] Systematic deviations between calculated and known enthalpies of formation are corrected by applying bond additive corrections leading to generally good agreements (within 1 kcal/mol) with entries in the ATcT.[25] CCSD(T)/CBS 0K energies were extrapolated from CCSD(T)/cc-pVDZ, CCSD(T)/cc-pVTZ and, if feasible, CCSD(T)/cc-pVQZ energies calculated on CBS-QB3 optimized structures. For several species G4 geometries were also use for the CCSD(T)/CBS calculations but no significant differences in the CCSD(T)/CBS results were found. Similarly, CCSD(T)/CBS 0K energies were also extrapolated

from CCSD(T)/aug-cc-pVDZ and CCSD(T)/aug-cc-pVTZ results and the differences to the CCSD(T)/CBS calculated with non-augmented basis sets were found to be small.

Since the G4 energies agreed well with the CCSD(T)/CBS data, high pressure rate coefficients of important reactions were calculated with transition state theory using the G4 data as input. Eckart tunneling corrections using the asymmetric potential are applied in all kinetic calculations. The rate coefficient for barrierless bond scission reactions were estimated from the reverse addition reaction. In the case of iPN, taking a value of 7×10^{12} cm^3 mol^{-1} s^{-1} for the association reaction leads together with the thermal equilibrium constant at G4 level to an A factor of 2×10^{16} s^{-1} for the bond scission reaction.

The Multiwell program[26] was used to generate pressure-dependent rate expressions for the thermal decomposition of iPN, its radical C_2JCONO_2, and for the chemically activated reaction $CH_3+NO_2 \rightarrow CH_3NO_2$. For iPN and its radical, the Lennard-Jones parameters σ_{LJ} = 5.2 Å and ε_{LJ} =520 K were used and He is taken as bath gas (σ_{LJ} = 2.55 Å and ε_{LJ} =10.22 K). The LJ parameters σ_{LJ} = 3.89 Å and ε_{LJ} = 197.0 K taken from Matsugi and Hiroumi[27] were utilized for CH_3NO_2. The exponential down model with $\langle E_{down} \rangle$ = 200 cm^{-1} was selected to describe the energy transfer by collisions. The number of trials and the time window for reaction were adapted based on the temperature investigated. For iPN decomposition, calculations were done for temperatures between 750 K and 1500 K and for its radical the temperature range was 500 K – 1500 K. The temporal decays of iPN or its radical can be described at the lowest temperatures by single exponential functions while non-exponential decays at higher temperature consist of a fast and a slow component. The slow decay rate is consistent with the exponential decay observed at the lower temperatures, while the fast decay describes the spontaneous decomposition of highly energized molecules. This bimodal behavior appeared at temperatures above 800 K hence beyond the maximum experimental temperature of this study. The reported rate expressions in this work describe the slow decay and the temperature ranges used for the fits are indicated in the corresponding table.

The chemical activation analysis of the $CH_3+NO_2 \rightarrow CH_3NO_2$ reaction with Multiwell yields the fraction of collisions that are deactivated to CH_3NO_2 instead of re-dissociating to the reactants. From these fractions as function of temperature and pressure, rate expressions for this channel can be calculated. The required high-pressure limit rate coefficient was taken from Glänzer and Troe,[28] increased by 10% to reflect the slightly higher predictions by Annesley et al.[29] A brief review of this reaction is provided in SM (see Figure S20).

3. Modeling

All simulations were performed with the plug flow module of the ANSYS Chemkin Release 17.2[30] assuming the validity of the plug flow approximation. Instead of providing an approximate residence time to the software, experimental inlet flow velocities were used for more accurate simulations. The measured (or interpolated) temperature profiles served as input data. Experimental inlet flow velocities and temperature profiles are provided in SM (Figure S1 and Table S1). In all figures showing model predictions, symbols represent the experimental data and lines represent the simulation results.

4. Kinetic Mechanisms

Four kinetic models were used to simulate the iPN pyrolysis data: the iPN mechanism by Fuller et al.,[19] the N mechanism for combustion by Glarborg et al.,[31] the mechanism by Mohamed et al.[32] used to study the impact of NOx on ethane oxidation and the nitromethane model presented by Shrestha et al..[21] Since the Glarborg, Mohamed and Shrestha mechanisms do not contain iPN chemistry, a small iPN submodel was added to those.

As mentioned before, the recent mechanism by Fuller et al.[19] is the only one available that was developed for iPN pyrolysis. It is created from several core mechanisms, which are the recently published C_0-C_3 theory-informed chemical kinetic model by Miller, Klippenstein and co-workers,[33] the nitrogen mechanism by Glarborg et al.[31] and the iPN chemistry optimized by Fuller et al.[11] Several updates and additions to these core mechanisms were made based on kinetics developed by Goldsmith and co-workers[34-37] and others.[29,38] The core reactions and updates are largely taken of very recent studies, hence this mechanism can be considered as current state of the art. It was solely released in Cantera[39] format and had to be converted to Chemkin format as part of this study. Regarding iPN reactions, the Fuller model only contains 2 (or 3) reactions: The bond scission reaction forming isopropoxy and nitrogen dioxide, the molecular channel forming acetone and nitrous acid and the same reaction formulated as roaming reaction. In the version of the Fuller mechanism used this roaming channel was set to zero, hence only two iPN reactions are active.

The second mechanism employed is the unmodified Glarborg nitrogen chemistry mechanism[31] which was provided as supporting material to the review article about nitrogen combustion chemistry. Except for iPN, isopropanol and isopropoxy, this Chemkin formatted mechanism contains all species that are expected to play a role in iPN pyrolysis at the conditions employed in the current study. However, it should be noted that the target of this mechanism is nitrogen combustion chemistry at higher temperatures than those explored in this study.

The third kinetic model was developed by Mohamed et al.[32] to simulate the impact of NOx on ethane oxidation. It is slightly updated from Sahu et al.,[40] who studied methane oxidation and ignition in the presence of NO_x. The core nitrogen chemistry is taken from Glarborg, but supplemented with hydrogen/syngas chemistry taken from Zhang et al.[41] and ab initio results. The use of NUIGMech1.2 as core hydrocarbon oxidation model causes this mechanism to be substantially larger than the previously discussed mechanisms, but also more comprehensive and well validated.

The final model tested is specifically adapted to reproduce nitromethane combustion experiments in jet-stirred and flow reactors. This kinetic model reported by Shrestha et al.[21] should be particular applicable to the experiments conducted in this current study if – as expected - the nitromethane sub-mechanism plays an important role. It is based on a previous model by the same group[42] to predict interactions between NO_x with methanol and ethanol oxidation chemistry. To this mechanism re-evaluated CH_3NO_2 chemistry was added.

Since the Glarborg, Shrestha and Mohamed mechanisms do not contain reactions of iPN, those were added with rate expressions derived from G4 calculations performed in the current study. The relevant parts of the potential energy surfaces (PES) for iPN and its terminal radical C_2JCONO_2 are shown in Figure 1. Note that "J" in the names of radicals denote the radical site. Furthermore, H atoms are omitted in this notation. Even though iPN has three reaction channels with comparable barrier heights, the bond scission completely dominates because the transition states of the two other channels are tight. Similarly, the transition state of the ring closure channel for C_2JCONO_2 radical is tighter than those of the two β-scission channels, which therefore dominate. The cyclic isomer may undergo many reactions (see a more complete PES in SM, Figure S14) but the channels leading to acetaldehyde, formaldehyde and nitric oxide are those with lowest overall barriers and in the MultiWell analysis these products have been assumed to be formed directly from the isomerization product. As shown in Figure S14 (SM), we considered additional C_2JCONO_2 decomposition reactions including β-scission reactions producing either CH_3 or H but also the formation of acetonyl and HONO, but the transition state energies for these channels are too high to play a role at low temperatures (500 K).

The bond dissociation energy (0 K) for iPN forming i-propoxy radical and nitrogen dioxide is calculated to be 41.3 kcal/mol at the G4 level of theory. This value agrees well with the UCCSD(T)-f12a/cc-pVTZf12//M11/jun-cc-pVTZ[43,44] value of 41.9 kcal/mol and the optimized value of 40.9 kcal/mol reported by Fuller et al. This good agreement is encouraging because the G4 calculations require substantially less computational resources. On the other hand, Fuller et al. calculate the barrier for acetone and nitrous acid to be 42.6 kcal/mol, which is clearly higher than the 41.2 kcal/mol result shown in Figure 1. The third channel to propene and nitric acid was not considered by Fuller et al.. In Table S4, we provide a comparison of these data with CBS-QB3 as well as various CCSD(T)/CBS

extrapolations, which further support the reliability (within 1 kcal/mol) of the G4 results for the chemistry relevant to this study.

The rate coefficients for the reactions on the two PES shown in Figure 1 were calculated with MultiWell software, which uses a stochastic method to analyze pressure-dependence. The results are given in

Table 1 and plots of the rate expressions as a function of pressure and temperature are provided in Figure S13. The rate expression for iPN dissociation at 750 K and 10 atm is already close to the high-pressure limit (shown as kTST in Figure S13) and for 1 atm the rate expression is approaching the high-pressure limit rapidly with decreasing temperature. Since iPN decomposes already around 500 K at the experimental conditions chosen in this study, the high-pressure limit rate expression would be sufficient to use. Table 1also contains rate coefficients for H abstraction from iPN. The product from H abstraction reactions from the tertiary C-H site formally yields the C_2CJONO_2 radical, which is not stable and immediately decomposes to acetone ($C_2C=O$) and NO_2. The reactions listed in

Table 1 are used to complement the kinetic mechanisms of Glarborg, Shrestha and Mohamed. Table S3 reports besides the geometries, frequencies, and rotational constants for iPN and C_2JCONO_2 also the NASA polynomials for these species that were used in the Chemkin calculations.

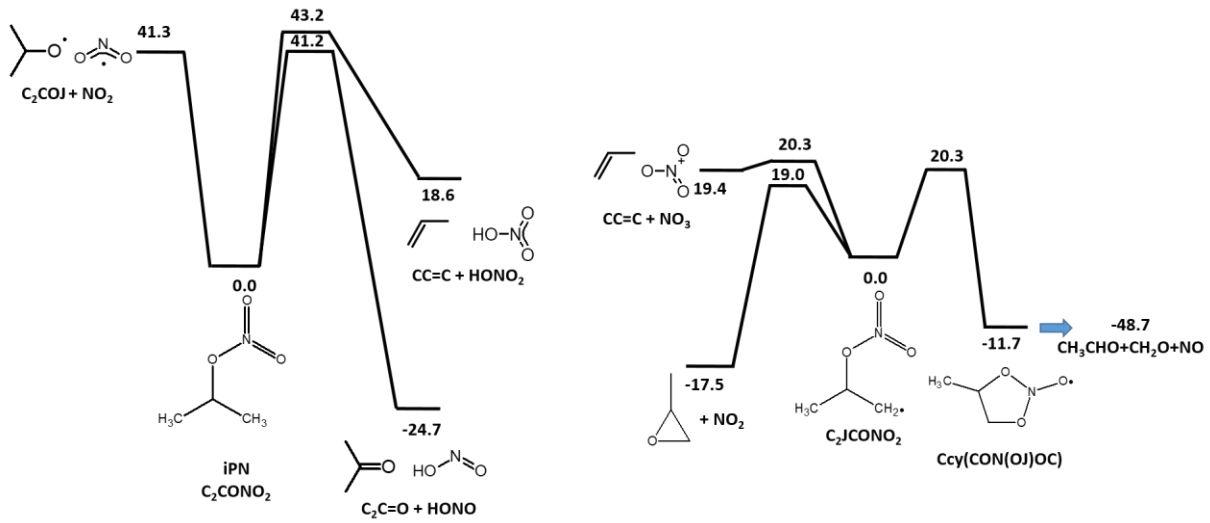

Figure 1: Simplified PES for iPN (left) and its radical C_2JCONO_2 (right) calculated at the G4 level of theory. All data are for 0K with ZPE correction and in kcal/mol. The "J" in the SMILES-like names indicate the radical site.

A comparison of the sizes of the four kinetic models (including iPN reactions) is given in Table 2. The kinetic model by Mohamed is substantially larger than the remaining mechanisms, since it contains the oxidation chemistry

of large hydrocarbon molecules. It thus has the potential to be more comprehensive than the other models regarding the secondary chemistry in iPN pyrolysis. On the other hand, the model by Shrestha contains the smallest number of species and might potentially lack chemistry of species with more than one carbon atom.

Table 1: Reactions and rate coefficients used for iPN sub-mechanism. The comments for pressure-dependent reactions include the temperature range, for which the modified Arrhenius parameters were fitted. "J" in larger radicals marks the radical site. M in the comment column is the collider. The structure of N-containing species is given in Table S2.

No	Reaction	P [atm]	k = A×T^n×exp(-E/RT) A, n, E values in units cm^3, s, mol, cal			comment
pressure-dependent reactions						
1	C_2CONO_2 => $C_2COJ+NO_2$	0.1	3.09×10^{78}	-20.01	58620.0	M = He; 750 K – 1100 K no more important channels
		1.0	1.89×10^{78}	-19.53	61150.0	
		10.	8×10^{77}	-18.95	64881.0	
2	C_2JCONO_2=> CC*C+NO_3	0.1	1.52×10^{-36}	13.789	-6121.0	M = He; 500 K – 850 K
		1.0	1.20×10^{02}	2.503	10266.0	
		10.	1.02×10^{28}	-5.034	22767.0	
3	C_2JCONO_2=> Ccy(COC)+NO_2	0.1	3.49×10^{-29}	11.465	-4168.0	M = He; 500 K – 850 K
		1.0	8.05×10^{-02}	3.374	8058.0	
		10.0	2.30×10^{27}	-4.969	21572.0	
4	C_2JCONO_2=> $CH_3CHO+CH_2O+NO$	0.1	1.14×10^{-22}	8.947	-1450.0	M = He; 500 K – 1100 K
		1.0	1.11×10^{05}	1.008	11063.0	
		10.	9.51×10^{49}	-12.229	32876.0	
H abstraction reactions						
5	$H+C_2CONO_2 = H_2+NO_2+C_2C*O$		9.0×10^{07}	1.80	5800.	this work
6	$H+C_2CONO_2 = H_2+C_2JCONO_2$		4.6×10^{07}	2.06	8600.	this work
7	$CH_3+C_2CONO_2 = CH_4+NO_2+C_2C*O$		1.6×10^{03}	2.80	7700.	this work
8	$CH_3+C_2CONO_2 = CH_4+C_2JCONO_2$		1.0×10^{03}	2.97	10200.	this work
9	$CH_3O+C_2CONO_2 = CH_3OH+NO_2+C_2C*O$		2.2×10^{05}	2.36	4100.	this work
10	$CH_3O+C_2CONO_2 = CH_3OH+C_2JCONO_2$		2.7×10^{03}	2.96	5800.	this work
11	$OH+C_2CONO_2 = H_2O+NO_2+C_2C*O$		2.3×10^{04}	2.62	-2000.	this work
12	$OH+C_2CONO_2 = H_2O+C_2JCONO_2$		4.6×10^{03}	3.03	500.	this work
13	$C_2COJ+CH_3CHO = C_2COH+CH_3CO$		2.2×10^{03}	2.75	-600.	this work
14	$C_2COJ+CH_2O = HCO+C_2COH$		4.7×10^{03}	2.82	1000.	this work
other reactions						
15	$C_2COJ = CH_3+CH_3CHO$		4.8×10^{13}	0.24	15000.	TST (no fall-off analysis)
16	C_2COJ => C_2C*O+H		3.0×10^{11}	0.75	17600.	

C_2CONO_2 = iPN, C_2JCONO_2 = radical of iPN, see Figure 1, C_2C*O = acetone, C_2COJ = isopropoxy radical, all other species names should be self-explaining

Table 2: Sizes of the kinetic models tested against the iPN pyrolysis data.

Mechanism	No species	No reactions	Reference
Fuller	152	1917	[19], converted to Chemkin format
Glarborg	158	1413	[31], augmented with iPN rxns
Mohamed	2866	11882	[32], augmented with iPN rxns
Shrestha	141	1212	[21], augmented with iPN rxns

Results and discussion

In this section of the paper are described the pyrolysis data obtained in the present work as well as the comparison with data computed with detailed kinetic models. A kinetic analysis is then performed to highlight specificities of the chemistry of iPN pyrolysis.

1. Experimental results and comparison with kinetic models

Profiles for selected species detected in the pyrolysis of iPN are shown in Figure 2. The mole fractions of all quantified species are provided in Table S4 and Figures S3 – S13 show additional profiles. Table S2 contains a list of all relevant species names and structures. Focusing first on the experimental data, Figure 1 clearly shows that iPN starts to decompose at temperatures at or even below 500 K and that within a narrow temperature window its consumption is total. As expected from Rxn 1 and Rxn 2, the decline of iPN is accompanied by a fast formation of acetaldehyde, since the initial bond scission product, isopropoxy (C_2COJ), is not stable at these temperatures and reacts dominantly via β-scission to acetaldehyde and methyl radical.

$iPN \rightarrow C_2COJ + NO_2$	D_RH^{298} = 42.3 kcal/mol	Rxn 1
$C_2COJ \rightarrow CH_3CHO + CH_3$	D_RH^{298} = -5.5 kcal/mol; barrier: 14.4 kcal/mol	Rxn 2

The acetaldehyde peak mole fraction reaches about 0.95 % of that of initial iPN. With a small delay and a somewhat less steep increase, formaldehyde is formed. While the GC and FTIR data are consistent at low temperatures, larger deviations of 30% reflect rather high uncertainties in the quantification of formaldehyde. Methanol formation seems to mirror the formaldehyde profile except that its concentration is about 50% less. Nitromethane (CH_3NO_2) is also rapidly produced – similar to formaldehyde and methanol – but its mole fraction only reaches a plateau value of a little above 0.002. Also interesting is the instantaneous increase of CO_2 at 500 K, however its maximum concentration is about one order of magnitude lower than that of nitromethane. The profiles of CO and NO increase more gradually suggesting that the formation of these products depends on secondary chemistry. Finally, given its toxicity, the detection of hydrogen cyanide at the highest temperatures with a significant mole fraction above 0.00025 is of importance. As shown in Figures S4-S6 other detected alkanes (CH_4, C_2H_6) and the alkene ethylene (C_2H_4) agree with the propene profile (Figure S7) in the sense that these species are largely produced at higher temperatures, hence their mole fraction profiles rise with increasing temperature. The profile of propene, however, is special because it contains

an initial increase around 550 K followed by a plateau region before the above-mentioned increase at the highest temperatures is observed.

All four models tested reproduce the rapid decay of iPN and increase of acetaldehyde (CH_3CHO) very well with modest differences between the G4 and the Fuller iPN chemistries. Recalling that all but the Fuller model contain the same iPN reaction subset, the similarity of all profiles from these models show that secondary chemistry does not have a notable impact of iPN consumption. Fuller et al. subjected their iPN reactions to an optimization step to best reproduce their experimental Schlieren profiles. The good agreement with the current iPN data demonstrates the transferability of their kinetic analysis. In this context it should be pointed out that the small uncertainties in the temperature profiles and flows prevent a clear decision, which iPN set reproduces the data best.

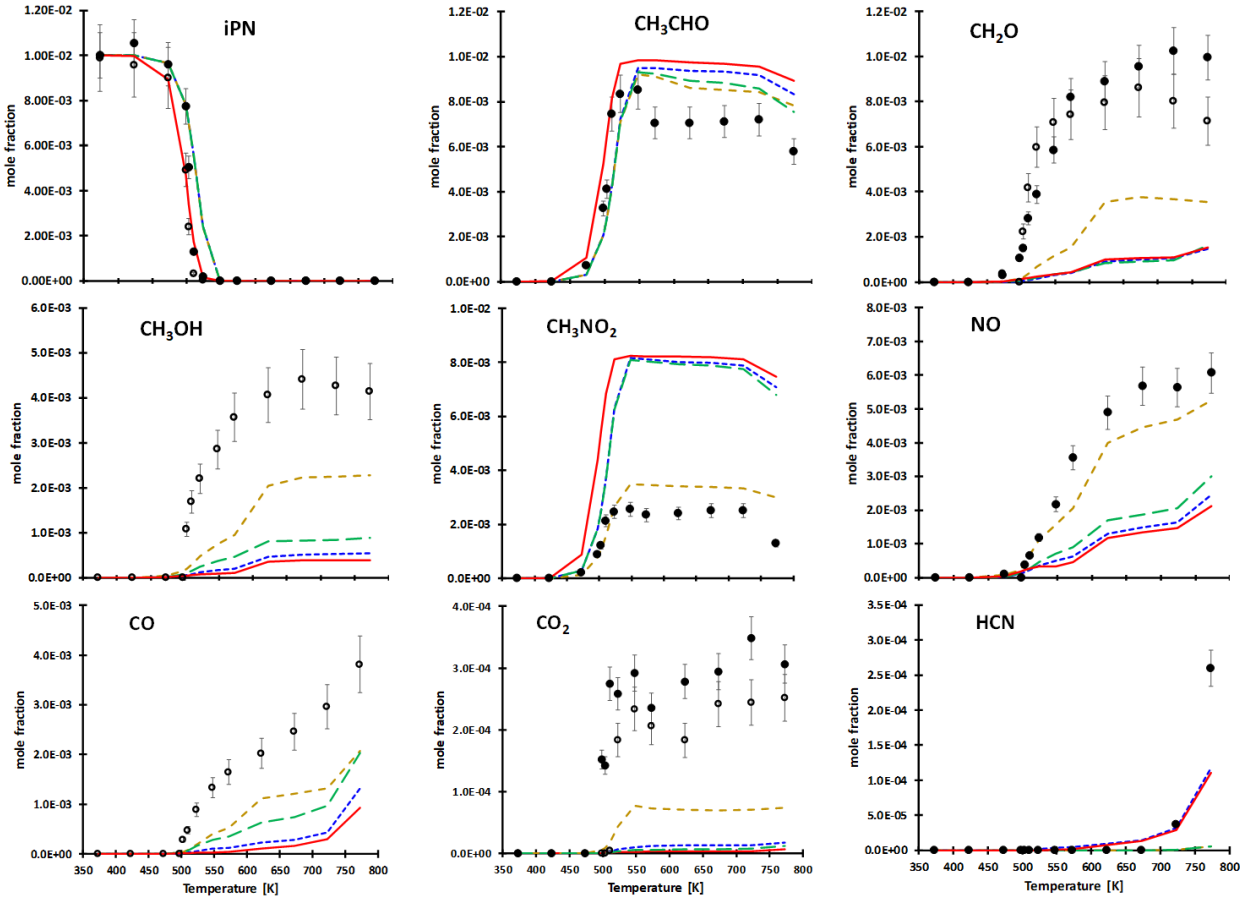

Figure 2: A comparison between experimental and predicted iPN decay and product formation profiles in the pyrolysis of 1% iPN in He in a flow tube reactor. Solid symbols: GC data; open symbols FTIR data; red solid line: Fuller model,[19] green long-dashed line: Shrestha based model;[21] blue short-dashed line: Glarborg based model;[31] brown dashed line: Mohamed based model.[32]

The most striking differences between experimental results and the different model predictions are observed for formaldehyde (CH_2O), methanol (CH_3OH) and nitromethane (CH_3NO_2). None of the models is able to reproduce the measured high yields of formaldehyde and methanol, however, unlike the other three models, the one by Mohamed predicts substantial formaldehyde and methanol formation, even though the absolute values are about a factor of two too low. Instead of methanol and formaldehyde production, the models by Fuller, Shrestha and Glarborg predict high yields of nitromethane, whereas the detected yields are more than a factor of three lower. The nitromethane profile simulated with the Mohamed model is only slightly higher than the experimental values, hence it again outperforms the other three models. The same holds for NO, which yields are slightly underpredicted by the Mohamed mechanism but in much better agreement compared to the alternative models (more than a factor of three underprediction at the lower temperatures). The Mohamed model also does reasonably well for the CO and CO_2 data, although both species are underpredicted. Only for the propene data, the Glarborg and Shrestha models preform as well, which indicates that propene is directly produced through reactions of the iPN subset. The simple two reaction sub-mechanism for iPN implemented in Fuller's model appears to be insufficient for the conditions of the current study.

2. Kinetic analysis

The objective of the following part is to identify the cause for the different performance of the Mohamed based model compared to the remaining models. After establishing a suitable condition for the rate analysis and the overall reactive flow, it will be shown that the reaction between methyl radicals and nitrogen dioxide plays an important role and that this chemistry is differently implemented in the Mohamed model compared to the others. Arguments are presented in support of the kinetics used by Mohamed. The kinetic models of Glarborg, Fuller and Shrestha are subsequently upgraded with results from a ME analysis for this reaction and improvements of the predictions with the modified models compared to the original results verify the importance of this reaction. One outcome of these comparisons is that additional modifications are needed to fully capture the experimental results. Based on rate analysis results, other reactions of importance for the production of the main quantified products are briefly discussed.

a. Rate of production and analyses of temporal profiles of key species

The kinetically most interesting temperature region is that between 525 - 550 K, since in this temperature range the yields of the major secondary products such as formaldehyde, methanol and nitromethane establish their final

plateau value. Therefore, the following kinetic analysis focuses on simulation results obtained at the nominal temperature of 548 K.

As can be seen from Figure 3, the chemistry in the tubular reactor starts clearly before the maximum temperature is reached and it comes to an end at the distance of maximum temperature after which the concentrations of the stable products remain unchanged and the radical concentrations are too low to be visible. The profiles predicted with the Fuller model are slightly shifted to shorter distances than those of the remaining models because it uses a different iPN decomposition chemistry. Given that the mole fractions for CH_3 and CH_3O peak around 20 cm, rate analyses were performed at this distance. The rate of production analysis for the Mohamed based model is shown in Figure 4.

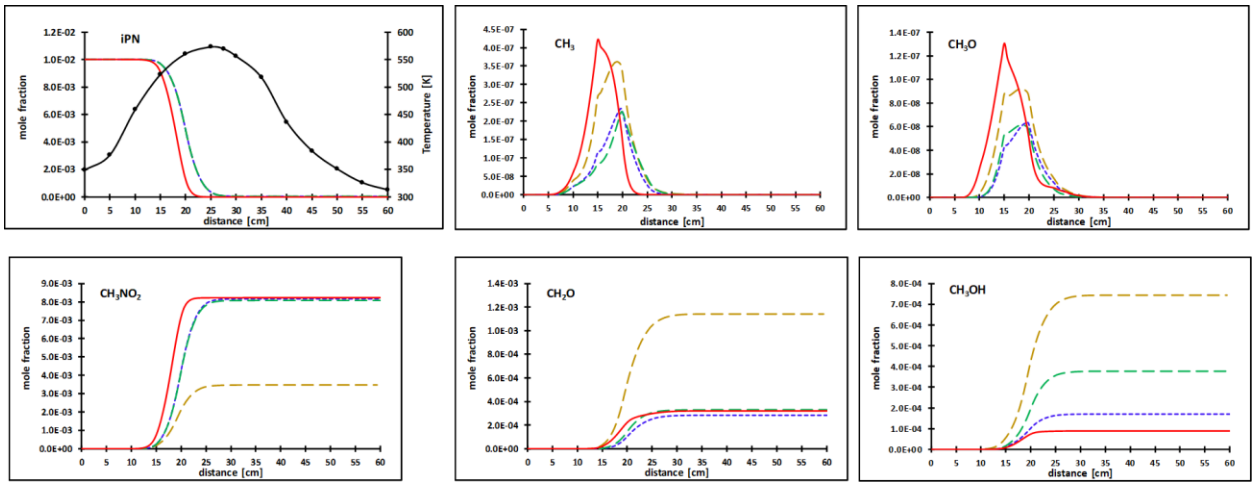

Figure 3:Temporal temperature and predicted species profiles for the T=548 K conditions. Black: experimental temperature profile. Red solid line: Fuller model,[19] green long-dashed line: Shrestha based model;[21] blue short-dashed line: Glarborg based model;[31] brown dashed line: Mohamed based model.[32]

The initial part of the flow diagram is commonly accepted: iPN like other alkyl nitrates mainly decompose unimolecularly. In the Fuller model, this is the only active channel in their model (the acetone and nitrous acid pathway does not notably contribute), since it was developed for the interpretation of Schlieren shock tube data. This explains why the Fuller mechanism does not predict propene formation, which is a product of C_2JCONO_2 decomposition (see Figure 1 (right)). Almost all isopropoxy (C_2COJ) decomposes via β-scission to acetaldehyde and methyl radical, but a small fraction undergoes abstraction reactions producing isopropanol as product, which has been detected and quantified in this study (see Figure S9). The majority of the methyl radicals (89.8%) created through isopropoxy decomposition react with NO_2 to either nitromethane (CH_3NO_2) or to methoxy and nitric oxide (NO). Both, methoxy and nitric oxide (or its hydrogenation product HNO) are involved in the formation of methanol, formaldehyde and methyl nitrite (CH_3ONO), while the reaction of methoxy with nitrogen dioxide produces methylnitrate (CH_3ONO_2).

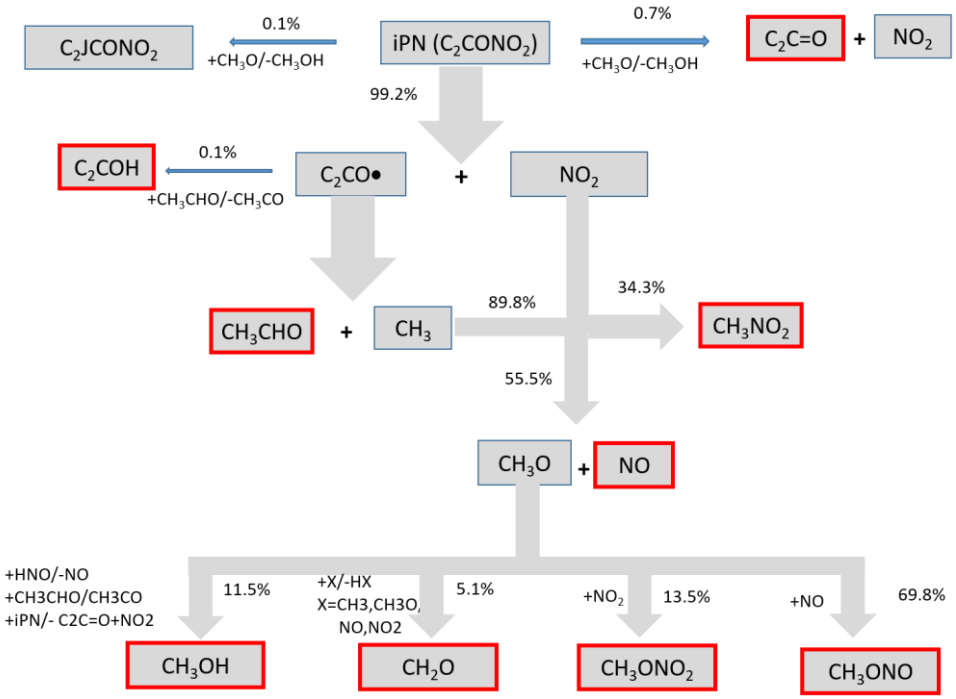

Figure 4: Rate of production analysis at 548 K and 20 cm distance using the Mohamed based mechanism. The species in red boxes have been quantified in this study.

Figure 5: CH_3 radical Rate of Production (ROP) analyses for the four kinetic models discussed in this work. The absolute fluxes differ, hence only the relative contributions are important. "C_2COJ" and "IC_3H_7O" are different names for the isopropoxy radical. The reaction labeled "CH_3NO_2 <=> CH_3+NO_2" in the Fuller model is pressure-dependent as it is in the other models, but the (+M) marker is missing because in that model the PLOG format is used.

A key difference between the Mohamed mechanism and the other three lies in the branching ratio between the two CH_3+NO_2 reaction channels. As can be seen in Figure 4, the Mohamed mechanism predicts the methoxy channel to

be more important than the nitromethane channel. Similar analyses with the other mechanism show that in those the nitromethane pathway is about five times faster than the methoxy channel (see Figure 5). Given the identified importance of the CH_3+NO_2 reaction, a more detailed analysis is presented next.

b. Kinetic analysis of the CH_3+NO_2 reaction

At the experimental conditions of this work and temperatures around 550 K, methyl radicals formed through β-scission of isopropoxy radicals are mainly consumed by its reaction with NO_2 (Figure 5). The rate coefficient used for the two important channels

$$CH_3+NO_2 \leftrightarrows CH_3O+NO \qquad \textit{Rxn 3}$$

and

$$CH_3+NO_2\,(+M) \leftrightarrows CH_3NO_2\,(+M) \qquad \textit{Rxn 4}$$

differ among the models. Rxn 3 is a chemically activated, pressure independent reaction with a rate coefficient around 1×10^{13} $cm^3mol^{-1}s^{-1}$. The left plot of Figure 6 shows that the Glarborg model uses a temperature independent rate coefficient while the other three model assume a small negative temperature dependence. The Mohamed model uses the fastest rate coefficient but at 550 K all rate expressions are within 30% equal.

In contrast, Rxn 4 is pressure-dependent, because the initial adduct, chemically activated $[CH_3NO_2]^*$, either re-dissociates or experiences collisional deactivation, which finally leads to thermalized CH_3NO_2. None of the kinetic models provide rate expressions for the forward reaction $CH_3+NO_2+M \rightarrow CH_3NO_2+M$, but instead the kinetic parameters are calculated from the reverse reaction, $CH_3NO_2+M \rightarrow CH_3+NO_2+M$. Consequently, the rate coefficient for Rxn 4 depends on a proper description

of the dissociation of nitromethane in the low temperature region studied here, in which nitromethane decomposes extremely slowly. In other words, the rate expression for CH_3NO_2 decomposition at 550 K relies heavily on an extrapolation from measurements at higher temperature. Furthermore, the rate expression for Rxn 4 requires thermodynamic data of the reactants and products, which are not the same for the four models tested. Finally, it is theoretically questionable whether the calculation of the reverse rate coefficient through thermal equilibrium is valid, because the fact that the reaction proceeds through a chemically activated intermediate implies that the energy distribution is not a Boltzmann distribution.

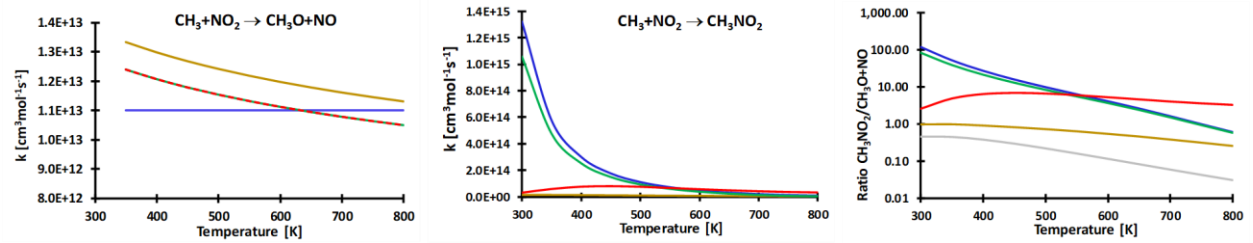

Figure 6: Left: Rate coefficients for Rxn 3 used by the four models. Central: Rate expressions for Rxn 4 used by the four models. Right: Ratios k(Rxn 3 / k(Rxn 4) at 1.07 atm. See text for explanations. The color code is the same as above (red: Fuller based model,[19] green: Shrestha based model;[21] blue: Glarborg based model;[31] brown: Mohamed model[32]). The grey line in the right plot is the ratio calculated from a MultiWell analysis as part of this work.

Using rate analyses for CH_3+NO_2 for temperatures between 350 K and 800 K allows to determine the flux ratio Rxn 3 / Rxn 4 for all four models. These ratios are shown in the right plots of Figure 6. The central part is calculated using these ratios and the rate coefficients for Rxn 3. This procedure is chosen because it does not require any assumption of how the rate coefficients for Rxn 4 are calculated by Chemkin.

The central and right-hand side plots of Figure 6 clearly indicate problems with the rate coefficients for Rxn 4 in the Glarborg and Shrestha models, because at low temperatures the rate expressions reach values beyond typical collision numbers of the order of 1×10^{14} $cm^3mol^{-1}s^{-1}$. Furthermore, a ratio of 10 or 100 for Rxn 3 / Rxn 4 is also unrealistic given the known high-pressure rate expressions for both reactions (see the brief discussion in the SM, p22). The curvature of the Fuller data is also questionable because the rate coefficient for Rxn 4 should increase with decreasing temperature (approaching the high-pressure limit) and therefore the ratio Rxn 3 / Rxn 4 should become relatively constant at low temperatures. Interestingly, at 500 - 550 K, the temperature region in which iPN decomposes and the primary final products are formed, the rate coefficients for Rxn 4 are very similar for these three models. The rate coefficients used by the Mohamed do not display obvious problems. The ratio Rxn 3 / Rxn 4 approaches a constant value and the value for the forward direction of Rxn 4 is within the range of the total collision number. Therefore, the analysis of the CH_3+NO_2 reaction supports the superior performance of this kinetic model.

In order to validate that a proper implementation of reactions Rxn 3 and Rxn 4 into the kinetic models of Glarborg, Shrestha and Fuller leads to improved predictions, one could simply use the CH_3+NO_2 kinetics by Mohamed. However, this would mean that the rate coefficients for Rxn 4 would have to be calculated through thermodynamic equilibrium. A better approach is to perform a Master Equation analysis of this system to determine the pressure-dependent rate expression for Rxn 4. This has been done in the current work. The results are plotted in Figure 7 and reported in Table 3 in PLOG format.

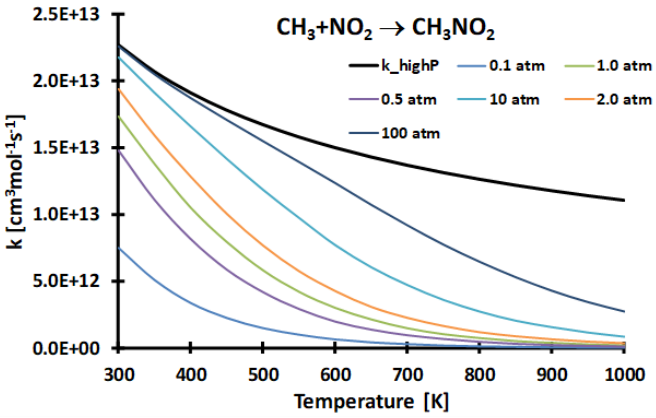

Figure 7: Pressure-dependent rate coefficients calculated with MultiWell.

Figure 7 clearly shows that Rxn 4 is in the fall-off region at the temperature range of interest (500 K and above). At 550 K and 1 atm, the value of the rate coefficients is only around 25% of that of the high-pressure limit. Furthermore (see Table 3), the methoxy and NO channel is at this temperature about five times faster according to the new calculation results.

Table 3: Recommended rate coefficients for the CH_3+NO_2 reactions Rxn 3 and Rxn 4. Format $k(T)=A\cdot T^n \cdot exp(-E/RT)$. A is given in $cm^3mol^{-1}s^{-1}$ and E is given in kcal/mol. Validity range: 300 K – 1000 K for bath gas helium.

Reaction	Rate coefficients (A, n, E)				k (550 K) [$cm^3mol^{-1}s^{-1}$]	comment
$CH_3+NO_2 \rightarrow CH_3O+NO$		5.33×10^{14}	-0.495	-0.009	2.36×10^{13}	Annesley[29,*]
$CH_3+NO_2 \rightarrow CH_3NO_2$	0.1 atm	4.56×10^{39}	-9.392	4.872	9.67×10^{11}	This work
	0.5 atm	5.24×10^{39}	-9.184	5.267	2.88×10^{12}	
	1 atm	1.86×10^{39}	-8.947	5.363	4.17×10^{12}	
	2 atm	4.60×10^{37}	-8.344	5.143	5.67×10^{12}	
	10 atm	1.57×10^{35}	-7.386	4.963	9.62×10^{12}	
	100 atm	8.00×10^{27}	-4.890	3.414	1.40×10^{13}	

* the rate coefficient was obtained by digitizing the plot in Figure 10 from ref [29], fitting to a modified Arrhenius expression and scaling by 0.89 to match the experimental data by Matsugi and Shiina[27] at higher temperatures.

Incorporation of the kinetics of Table 3 into the Glarborg, Shrestha and Fuller model leads to clearly observable improvements of the predictions of several major species such as formaldehyde, methanol, nitromethane and NO (Figure 8). Methylnitrite is now over-predicted, but this might be caused by the same problem discussed above for Rxn 4, namely that the rate expressions for the pressure-dependent thermal decomposition of methylnitrite are not directly incorporated in the tested models but calculated through thermal equilibrium. It should also be pointed out, that the agreements are far from perfect and future studies would be desirable to further improve the models. Nevertheless, the observed progress creates confidence in the kinetic analysis of this work.

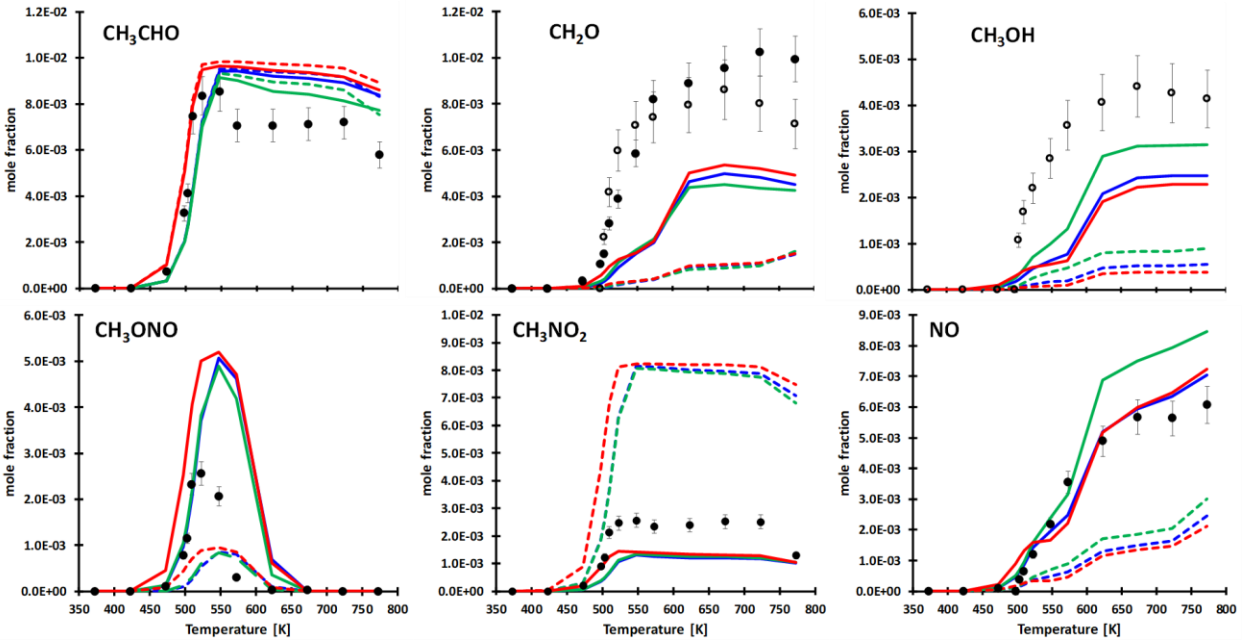

Figure 8: Improved performance of the Glarborg (blue), Shrestha (green) and Fuller (red) based models after implementing the kinetic data presented in Table 3. Full lines present predictions with the updated mechanisms, dotted lines: original mechanisms.

c. Other, important reactions of the experimentally observed species.

In this part, important reactions other than the CH_3+NO_2 recombination are briefly discussed in the context of the formation the observed species.

As discussed above and well established in the literature, ***iPN*** like other alkyl nitrates is dominantly consumed by the homolytic rupture of the C_2CO—NO_2 bond. But this not the only important consumption reaction. A small fraction of iPN is consumed through H abstraction reactions e.g. by CH_3O and CH_3 radicals, as evidenced by the detection of ***propene***, ***acetone, isopropanol*** and methane. Propene could also be formed through molecular elimination from iPN itself, but the lack of propene formation by the Fuller model, which does not include the abstraction reactions but only the molecular pathway, strongly supports the importance of abstraction reactions. Acetone may also result from the minor β-scission channel of isopropoxy radicals (Rxn 5),

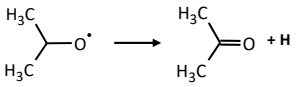

Rxn 5

and the rate analyses with the four tested models show that both reactions are important.

Acetaldehyde is produced from the main β-scission pathway of isopropoxy radicals (see Figure 4). More interesting is its consumption. All four kinetic models predict acetaldehyde to be relatively unreactive except for the highest temperatures. In contrast, the experimental data suggests that about 15 % of it is consumed shortly after iPN consumption is completed. A possible reaction responsible for acetaldehyde consumption could be Rxn 6:

$$CH_3O + CH_3CHO \rightarrow CH_3OH + CH_3CO \qquad \textit{Rxn 6}$$

An update of the CH_3+NO_2 reaction leads to higher methoxy yields and this would accelerate this reaction. A sensibility analysis using the Mohamed model identifies this reaction as the most important consumption step.

The yield of ***nitromethane***, CH_3NO_2, is directly related to the CH_3+NO_2 branching ratio and any variation towards higher CH_3O+NO yields will also address the severe over-prediction of nitromethane by all but the Mohamed model. This is shown in Figure 8, in which the predicted CH_3NO_2 yields are reduced after updating the models with the new CH_3+NO_2 chemistry. The decline of CH_3NO_2 caused by thermal decomposition is well captured by all models. Similar to nitromethane, the ***nitrogen monoxide*** (NO) yield predictions depend on the correct branching ratio of the CH_3+NO_2 reaction. Consequently, NO is well predicted by the Mohamed model and severely underpredicted by the other models. Upon upgrading, these latter models perform much better. The NO reactions Rxn 7,

$$CH_3 + NO + M \rightarrow CH_3NO + M \qquad \textit{Rxn 7}$$

and Rxn 8,

$$CH_3O + NO + M \rightarrow CH_3ONO + M \qquad \textit{Rxn 8}$$

contribute most to its consumption at 550 K. Consistent with the kinetic analysis discussed above, the experimental ***methyl nitrite*** (CH_3ONO) profile is well reproduced by the Mohamed model, while the other models severely underpredict the yields (Figure S3 in SM). After updating the CH_3+NO_2 reaction, methyl nitrite is overpredicted (Figure 8). The broader predicted profiles suggest that methyl nitrite decomposition might need to be revised in a similar way as the CH_3+NO_2 reaction.

The ***CO*** and ***CO_2*** yields predicted by any model are lower than those measured experimentally. This is consistent with the lack of acetaldehyde consumption mentioned above, because the most important CO formation reaction is Rxn 9,

$$CH_3CO + M \rightarrow CH_3 + CO + M \qquad \textit{Rxn 9}$$

Similarly, the most important CO_2 formation pathway (Rxn10),

$$CH_3CO + NO_2 \rightarrow CH_3 + CO_2 + NO \qquad \textit{Rxn 10}$$

also depends on acetyl (CH_3CO). Improvements of acetaldehyde predictions thus should simultaneously improve the results for both, CO and CO_2.

Among the minor species, only four species will be discussed here. The formation of small quantities of ***isopropanol***, C_2COH, suggests that its radical, C_2COJ, formed through iPN decomposition, does not completely decompose to acetaldehyde + methyl, but a small part seems to participate in abstraction reactions. The rate analysis shows the dominance of the reaction Rxn 11

$$C_2COJ + CH_3CHO \rightarrow C_2COH + CH_3CO \qquad \textit{Rxn 11}$$

in all but the Fuller model. Latter does not contain C_2COH chemistry. In this context it is important to note that the C_2COH peak around 500 K might not be reproduced by any model because the reaction Rxn 12

$$C_2COJ + iPN \rightarrow C_2COH + products \qquad \textit{Rxn 12}$$

is missing.

Hydrogen cyanide, HCN, stands out due to its toxicity. All models predict its formation at the higher temperature range. One reaction important in all models is Rxn 13:

$$CH_3 + NO \rightarrow HCN + H_2O \qquad \textit{Rxn 13}$$

Experimental data on water production at higher temperatures might be helpful to validate this channel, but water is difficult to quantify and it is also produced by other reactions.

Finally, the experimental detection of ***formamide*** ($HCONH_2$) and ***acetamide*** (CH_3CONH_2) needs to be addressed. The identification of formamide is based on the match of its mass spectrum with the database spectrum. Due to similar features of the mass spectrum, the C_3H_5NO species is assigned as acetamide. Both assignments are firm and leave little room for incorrect identifications. However, none of the kinetic models predicts notable amounts of these compounds. Formamide is the lowest energy isomer of nitrosomethane, CH_3NO. Similarly, acetamide is an isomer of nitrosoethane. Both, nitrosomethane and nitrosoethane yields are predicted by the models and the nitrosomethane of the simulations agrees in shape well with the experimental formamide profile (grey lines in Figure S8). Since no low–energy gas phase reactions are known to convert these isomers at the low temperatures studied, one might speculate that heterogeneous reactions in the transfer line or analysis section could be responsible for the detection of these amides.

Conclusions

The pyrolysis of iPN was studied in a tubular reactor at temperatures between 373 and 773 K and a residence time of ~2 s in the hot zone. The initial iPN mole fraction was 0.01, diluted in helium, and the pressure was 1.07 atm. The main reactivity is observed at temperatures between 500 K and 550 K. Within this temperature region, the formation of high yields of acetaldehyde, formaldehyde, methanol, and nitromethane is observed. Other species detected are

methane, CO, NO, NO_2, formamide, methyl nitrate, methyl nitrite, acetone, H_2O, CO_2, ethane, isopropyl alcohol, ethylene, propene, acetamide and HCN.

Four literature kinetics models containing considerably large nitrogen sub-mechanisms, three of them augmented with a few iPN related reactions, were used to simulate the experimental data. All models predict the consumption of iPN and the formation of acetaldehyde well. None of the models was able to fully explain the high yields in formaldehyde and methanol, but the predictions with the model of Mohamed et al.,[32] augmented with iPN chemistry, are clearly superior to those with the other models. This is explained with a different branching ratio of the CH_3+NO_2 reaction, which has been identified as a crucial step. In the Mohamed model, the $CH_3+NO_2 \rightarrow CH_3O+NO$ dominates in the 500 K – 550 K range while the other three favor the $CH_3+NO_2 \rightarrow CH_3NO_2$ channel. The iPN pyrolysis experiments thus provide a severe test for this reaction, although it alone does not fully account for the discrepancy between model predictions and experimental results. Additional work is needed to identify other (and possibly missing) reactions that also play an important role in this system.

A further analysis of the CH_3+NO_2 reaction leads to the conclusion that the implementation of the $CH_3+NO_2 \rightarrow CH_3NO_2$ channel through the formally reverse reaction, $CH_3NO_2+M \rightarrow CH_3+NO_2+M$ creates a high level of uncertainty not only because of the extrapolation to the low temperatures used in this study, but the question is raised if the calculation of the rate coefficient for the reverse reaction through chemical equilibrium is valid, since it is a pressure-dependent reaction. The idea of using an alternative implementation of this reaction by making the $CH_3NO_2+M \rightarrow CH_3+NO_2+M$ reaction irreversible and separately adding rate information for the $CH_3+NO_2+M \rightarrow CH_3NO_2+M$ obtained from a MultiWell analysis was tested and lead to improved simulation results even though there is room for further improvements.

The detection (and prediction) of HCN at the highest temperatures studied points to potential health issues when using iPN and other nitrates are fuel additives. Therefore, it would be interesting to investigate if HCN is also formed at mixed fuel conditions.

The iPN experiments performed in this study proved to provide challenging data for the some of the best nitrogen models available in the literature. Unfortunately, the uncertainties in the data are quite high as evidenced by the poor elemental balances, the highly non-isothermal temperature profiles, the missing quantifications of important species, such as water, molecular hydrogen and nitrogen and the puzzling detection of formamide and acetamide. This calls for new experimental studies to further improve the available experimental database in this interesting low temperature region and to provide even more stringent test cases for the best available kinetic mechanisms for nitrogen chemistry.

Supporting Information

This manuscript is accompanied by:

- A file containing additional information (Temperature profiles; Elemental balances ; List of names and structures of nitrogen containing species; Geometries, frequencies, rotational constants and NASA polynomials for iPN and its radical C_2JCONO_2; Experimental results and model comparisons; Pressure-dependent rate coefficients for iPN decomposition; Ab initio energies related to iPN and CH_3NO_2; PES of C_2JCONO_2; Pressure-dependent rate expressions for unimolecular decomposition of the iPN radical $CH_3C(H)(ONO_2)CH_2$, labelled C_2JCONO_2; High-pressure limit rate coefficients for $CH_3NO_2 \rightarrow CH_3+NO_2$; Brief review of the High-pressure limit rate coefficients for the reactions $CH_3+NO_2 \rightarrow CH_3O+NO$ and $CH_3+NO_2 \rightarrow CH_3NO_2$).
- Mechanism files under Chemkin format.
- Input files used with the Multiwell program to generate pressure-dependent rate expressions.

Acknowledgments

The experimental work on iPN pyrolysis has been supported by TERBIS, 943 rue Pasteur, 60700 Pont-Sainte-Maxence, France. MUA and HHC acknowledge funding through the Project RTI2018-098856-B-I00 financed by MCIN/AEI/10.13039/501100011033/FEDER "Una manera de hacer Europa" and the Aragón Government (Ref. T22_20R), cofounded by FEDER 2014-2020 "Construyendo Europa desde Aragón". The authors are grateful to Guillaume Vanhove for his help in converting the Cantera format model from ref. 19 into Chemkin format.

Present adress: #N.V.: IFP Energies Nouvelles, Solaize, 69360, France

References

(1) Ambekar, A.; Chowdhury, A.; Challa, S.; Radhakrishna, D. Droplet Combustion Studies of Hydrocarbon-Monopropellant Blends. Fuel 2014, 115, 697–705.
(2) Suppes, G. J.; Rui, Y.; Rome, A. C.; Chen, Z. Cetane-Improver Analysis and Impact of Activation Energy on the Relative Performance of 2-Ethylhexyl Nitrate and Tetraethylene Glycol Dinitrate. Ind. Eng. Chem. Res. 1997, 36 (10), 4397–4404.
(3) Mbugua, A.; Satija, A.; Lucht, R. P.; Bane, S. Ignition and Combustion Characterization of Single Nitromethane and Isopropyl Nitrate Monopropellant Droplets under High-Temperature and Quasi-Steady Conditions. Combust. Flame 2020, 212, 295–308.
(4) Oxley, J. C.; Smith, J. L.; Rogers, E.; Ye, W.; Aradi, A. A.; Henly, T. J. Heat-Release Behavior of Fuel Combustion Additives. Energy Fuels 2001, 15 (5), 1194–1199.
(5) Kirsch, L. J.; Rosenfeld, J. L. J.; Summers, R. Studies of Fuel Injection into a Rapid Compression Machine. Combust. Flame 1981, 43, 11–21.

(6) Vin, N. Étude Cinétique de La Pyrolyse En Phase Gazeuse de Molécules Organiques Contenant Des Hétéroatomes Représentatives de Composés Toxiques Présents Dans Les Sols Pollués. These de doctorat, Université de Lorraine, 2019.
(7) Jullien, J.; Pechine, J.-M.; Perez, F.; Sadek, M. A. Décomposition Thermique En Phase Gazeuse Du Nitrate d'isopropyle. Propellants Explos. Pyrotech. 1983, 8 (4), 99–101.
(8) Zaslonko, I. S.; Smirnov, V. N.; Tereza, A. M. High-Temperature Decomposition of Methyl, Ethyl, and Isopropyl Nitrates in Shock Waves. High-Temp. Decompos. Methyl Ethyl Isopropyl Nitrates Shock Waves 1993, 34 (4), 531–538.
(9) Toland, A.; Simmie, J. M. Ignition of Alkyl Nitrate/Oxygen/Argon Mixtures in Shock Waves and Comparisons with Alkanes and Amines. Combust. Flame 2003, 132 (3), 556–564.
(10) Borisov, A. A.; Troshin, K. Y.; Mikhalkin, V. N. Ignition and Combustion of Isopropyl Nitrate. Russ. J. Phys. Chem. B 2016, 10 (5), 780–784.
(11) Fuller, M. E.; Goldsmith, C. F. Shock Tube Laser Schlieren Study of the Pyrolysis of Isopropyl Nitrate. J. Phys. Chem. A 2019, 123 (28), 5866–5876.
(12) Beeley, P.; Griffiths, J.; Gray, P. Rapid Compression Studies on Spontaneous Ignition of Isopropyl Nitrate .1. Non-Explosive Decomposition, Explosive Oxidation and Conditions for Safe Handling. Combust. Flame 1980, 39 (3), 255–268.
(13) Beeley, P.; Griffiths, J. F.; Gray, P. Rapid Compression Studies on Spontaneous Ignition of Isopropyl Nitrate Part II: Rapid Sampling, Intermediate Stages and Reaction Mechanisms. Combust. Flame 1980, 39 (3), 269–281.
(14) Griffiths, J.; Gilligan, M.; Gray, P. Pyrolysis of Isopropyl Nitrate .1. Decomposition at Low-Temperatures and Pressures. Combust. Flame 1975, 24 (1), 11–19.
(15) Griffiths, J.; Gilligan, M.; Gray, P. Pyrolysis of Isopropyl Nitrate .2. Decomposition at High-Temperatures and Pressures. Combust. Flame 1976, 26 (3), 385–393.
(16) Hansson, T.; Pettersson, J. B. C.; Holmlid, L. A Molecular Beam Mass-Spectrometric Study of Isopropyl Nitrate Pyrolysis Reactions at Short Residence Times and Temperatures up to 700 K. J. Chem. Soc. Faraday Trans. 2 Mol. Chem. Phys. 1989, 85 (9), 1413–1423.
(17) Morin, J.; Bedjanian, Y. Thermal Decomposition of Isopropyl Nitrate: Kinetics and Products. J. Phys. Chem. A 2016, 120 (41), 8037–8043.
(18) Powling, J.; Smith, W. A. W. Flame Decomposition of the Propyl Nitrates. Combust. Flame 1957, 1 (3), 308–320.
(19) Fuller, M. E.; Mousse-Rayaleh, A.; Chaumeix, N.; Goldsmith, C. F. Laminar Flame Speeds and Ignition Delay Times for Isopropyl Nitrate and Propane Blends. Combust. Flame 2022, 242, 112187.
(20) Phillips, L. Thermal Decomposition of Organic Nitrates. Nature 1947, 160 (4074), 753–754.
(21) Shrestha, K. P.; Vin, N.; Herbinet, O.; Seidel, L.; Battin-Leclerc, F.; Zeuch, T.; Mauss, F. Insights into Nitromethane Combustion from Detailed Kinetic Modeling – Pyrolysis Experiments in Jet-Stirred and Flow Reactors. Fuel 2020, 261, 116349.
(22) Vin, N.; Battin-Leclerc, F.; Herbinet, O. A Study of Thermal Decomposition of Bromoethane. J. Anal. Appl. Pyrolysis 2018, 136, 199–207.
(23) Frisch, M. J.; Trucks, G. W.; Schlegel, H. B.; Scuseria, G. E.; Robb, M. A.; Cheeseman, J. R.; Scalmani, G.; Barone, V.; Petersson, G. A.; Nakatsuji, H.; et al.; Revision B.01 ed.; Gaussian, Inc., Wallingford CT: 2016.
(24) East, A. L. L.; Radom, L. Ab Initio Statistical Thermodynamical Models for the Computation of Third-Law Entropies. J. Chem. Phys. 1997, 106 (16), 6655–6674.
(25) Ruscic, B. In McGraw-Hill Yearbook of Science & Technology 2005; McGraw-Hill: New York, 2004, p 3.
(26) Barker, J. R.; Nguyen, T. L.; Stanton, J. F.; Aieta, C.; Ceotto, M.; Gabas, F.; Kumar, T. J. D.; Li, C. G. L.; Lohr, L. L.; Maranzana, A.; et al.: University of Michigan, Ann Arbor, Michigan, USA, 2017.
(27) Matsugi, A.; Shiina, H. Thermal Decomposition of Nitromethane and Reaction between CH3 and NO2. J. Phys. Chem. A 2017, 121 (22), 4218–4224.
(28) Glänzer, K.; Troe, J. Reactions of Alkyl Radicals in the Shock Wave-Induced Pyrolysis of Nitroalkanes. Berichte Bunsenges. Für Phys. Chem. 1974, 78 (2), 182–184.
(29) Annesley, C. J.; Randazzo, J. B.; Klippenstein, S. J.; Harding, L. B.; Jasper, A. W.; Georgievskii, Y.; Ruscic, B.; Tranter, R. S. Thermal Dissociation and Roaming Isomerization of Nitromethane: Experiment and Theory. J. Phys. Chem. A 2015, 119 (28), 7872–7893.
(30) ANSYS, Inc.: San Diego, 2016.
(31) Glarborg, P.; Miller, J. A.; Ruscic, B.; Klippenstein, S. J. Modeling Nitrogen Chemistry in Combustion. Prog. Energy Combust. Sci. 2018, 67, 31–68.
(32) Mohamed, A. A. E.-S.; Panigrahy, S.; Sahu, A. B.; Bourque, G.; Curran, H. The Effect of the Addition of Nitrogen Oxides on the Oxidation of Ethane: An Experimental and Modelling Study. Combust. Flame 2022, 241, 112058.

(33) Miller, J. A.; Sivaramakrishnan, R.; Tao, Y.; Goldsmith, C. F.; Burke, M. P.; Jasper, A. W.; Hansen, N.; Labbe, N. J.; Glarborg, P.; Zádor, J. Combustion Chemistry in the Twenty-First Century: Developing Theory-Informed Chemical Kinetics Models. Prog. Energy Combust. Sci. 2021, 83, 100886.
(34) Chen, X.; Franklin Goldsmith, C. Predictive Kinetics for the Thermal Decomposition of RDX. Proc. Combust. Inst. 2019, 37 (3), 3167–3173.
(35) Chai, J.; Goldsmith, C. F. Rate Coefficients for Fuel+NO_2: Predictive Kinetics for HONO and HNO_2 Formation. Proc. Combust. Inst. 2017, 36 (1), 617–626.
(36) Labbe, N. J.; Sivaramakrishnan, R.; Goldsmith, C. F.; Georgievskii, Y.; Miller, J. A.; Klippenstein, S. J. Weakly Bound Free Radicals in Combustion: "Prompt" Dissociation of Formyl Radicals and Its Effect on Laminar Flame Speeds. J. Phys. Chem. Lett. 2016, 7 (1), 85–89.
(37) Labbe, N. J.; Sivaramakrishnan, R.; Goldsmith, C. F.; Georgievskii, Y.; Miller, J. A.; Klippenstein, S. J. Ramifications of Including Non-Equilibrium Effects for HCO in Flame Chemistry. Proc. Combust. Inst. 2017, 36 (1), 525–532.
(38) Rissanen, M. P.; Arppe, S. L.; Eskola, A. J.; Tammi, M. M.; Timonen, R. S. Kinetics of the R + NO_2 Reactions (R = i-C_3H_7, n-C_3H_7, s-C_4H_9, and t-C_4H_9) in the Temperature Range 201−489 K. J. Phys. Chem. A 2010, 114 (14), 4811–4817.
(39) Goodwin, D. G.; Moffat, H. K.; Schoegl, I.; Speth, R. L.; Weber, B. W. Cantera: An Object-Oriented Software Toolkit for Chemical Kinetics, Thermodynamics, and Transport Processes; Zenodo, 2022.
(40) Sahu, A. B.; Mohamed, A. A. E.-S.; Panigrahy, S.; Saggese, C.; Patel, V.; Bourque, G.; Pitz, W. J.; Curran, H. J. Combustion and Flame 2022, 238, 111746.
(41) Zhang, Y.; Mathieu, O.; Petersen, E. L.; Bourque, G.; Curran, H. J. Assessing the Predictions of a NOx Kinetic Mechanism on Recent Hydrogen and Syngas Experimental Data. Combust. Flame 2017, 182, 122–141.
(42) Shrestha, K. P.; Seidel, L.; Zeuch, T.; Mauss, F. Kinetic Modeling of NOx Formation and Consumption during Methanol and Ethanol Oxidation. Combust. Sci. Technol. 2019, 191 (9), 1627–1659.
(43) Peverati, R.; Truhlar, D. G. Improving the Accuracy of Hybrid Meta-GGA Density Functionals by Range Separation. J. Phys. Chem. Lett. 2011, 2 (21), 2810–2817.
(44) Adler, T. B.; Knizia, G.; Werner, H.-J. A Simple and Efficient CCSD(T)-F12 Approximation. J. Chem. Phys. 2007, 127 (22), 221106.

TOC figure